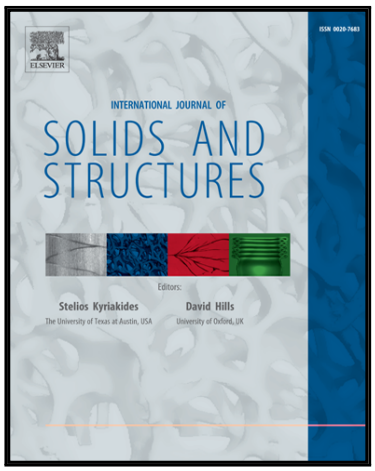

Effective elastic properties of composites with particles of polyhedral shapes

Anton Trofimov , Borys Drach , Igor Sevostianov

PII: S0020-7683(17)30194-4
DOI: 10.1016/j.ijsolstr.2017.04.037
Reference: SAS 9560

To appear in: *International Journal of Solids and Structures*

Received date: 16 February 2017
Revised date: 24 April 2017
Accepted date: 29 April 2017

Please cite this article as: Anton Trofimov , Borys Drach , Igor Sevostianov , Effective elastic properties of composites with particles of polyhedral shapes, *International Journal of Solids and Structures* (2017), doi: 10.1016/j.ijsolstr.2017.04.037

Effective elastic properties of composites with particles of polyhedral shapes

Anton Trofimov(raul_90@nmsu.edu)[a], Borys Drach (borys@nmsu.edu)[a]*,
Igor Sevostianov (igor@nmsu.edu)[a]

[a] Department of Mechanical and Aerospace Engineering, New Mexico State University, Las Cruces, NM

***Corresponding author:**
Borys Drach, Mechanical & Aerospace Engineering
P.O. Box 30001 / MSC 3450, New Mexico State University, Las Cruces, NM, USA 88003-8001
phone: +1 (575) 646-8041; fax: +1 (575) 646-6111; e-mail: borys@nmsu.edu

ABSTRACT

Contributions of 15 convex polyhedral particle shapes to the overall elastic properties of particle-reinforced composites are predicted using micromechanical homogenization and direct finite element analysis approaches. The micromechanical approach is based on the combination of the stiffness contribution tensor (N-tensor) formalism with Mori-Tanaka and Maxwell homogenization schemes. The second approach involves FEA simulations performed on artificial periodic representative volume elements containing randomly oriented particles of the same shape. The results of the two approaches are in good agreement for volume fractions up to 30%. Applicability of the replacement relation interrelating N-tensors of the particles having the same shape but different elastic constants is investigated and a shape parameter correlated with the accuracy of the relation is proposed. It is concluded that combination of the N-tensor components of the 15 shapes presented for three values of matrix Poisson's ratios with the replacement relation allows extending the results of this paper to matrix/particle material combinations not discussed here.

Keywords: polyhedral particles; homogenization; effective elastic properties; Mori-Tanaka; Maxwell; stiffness contribution tensor; periodic RVE; finite element analysis; micromechanics; replacement relation

1. Introduction

Regular polyhedra can be used to describe shapes of some crystalline metallic particles that are encountered as precipitates or synthesized as powders to be used as additives in particle-reinforced composites (Sundquist (1964), Menon and Martin (1986), Wang (2000), Onaka et al. (2003), Miyazawa et al. (2012), Niu et al. (2009)). Table 1 presents microscopy images of particles having polyhedral shapes along with their idealized shapes.

In this study, we analyze the effect of shape of several representative convex polyhedral on the overall elastic properties of particle-reinforced composites. Traditionally, the effect of inhomogeneities on elastic properties of materials is described using the classical Eshelby (1957) and Eshelby (1961) results for an ellipsoidal inhomogeneity. It means that the shape of the inhomogeneities is explicitly or implicitly assumed to be ellipsoidal (in most cases – just spherical). Few results on inhomogeneities having irregular geometry have been published in literature. In 2D, general cases of pores and inhomogeneities of arbitrary irregular shape have been studied using conformal mapping approach, see for example Zimmerman (1986), Jasiuk et al. (1994), Tsukrov and Novak (2002), Tsukrov and Novak (2004), Ekneligoda and Zimmerman (2006), Ekneligoda and Zimmerman (2008), Mogilevskaya and Nikolskiy (2015).

In 3D, several results for contributions of irregularly shaped inhomogeneities to effective elastic properties exist. Solutions for cracks having irregular shape are presented in Kachanov and Sevostianov (2012). Effect of concavity factor of superspheres and axisymmetric concave pores has been analyzed in the works of Sevostianov et al. (2008), Sevostianov and Giraud (2012), Chen et al. (2015) and Sevostianov et al. (2016). The authors supplemented finite element analysis (FEA) calculations with analytical approximations for compliance contribution tensors of pores of such shapes. The possibility to extend the results from pores to inhomogeneities with arbitrary properties has been discussed by Chen et al (2017). The authors showed that replacement relations (Sevostianov and Kachanov (2007)) that allow calculation of the compliance contribution tensor of an inhomogeneity from the one of a pore of the same shape are applicable to convex inhomogeneities only. Concave inhomogeneities require direct calculation of property contribution tensors. Drach et al. (2011) used FEA calculations to obtain compliance contribution tensors of several 3D irregularly shaped pores typical for carbon-carbon composites, and Drach et al. (2016) presented numerically obtained compliance contribution

tensors of cubical, octahedral and tetrahedral pores. Garboczi and Douglas (2012) presented a procedure to approximate bulk and shear elastic contribution parameters in the case of randomly oriented inhomogeneities shaped as blocks.

The effect of shape of an irregular inhomogeneity can also be analyzed by considering representative volume elements (RVEs) containing arrangements of inhomogeneties with orientation distribution of interest (e.g. random or aligned in the same direction). Rasool and Böhm (2012) analyzed contributions of spherical, cubical, tetrahedral and octahedral inhomogeneities to the effective thermoelastic properties of particle-reinforced composites with random particulate orientations. The results were obtained for the material combination with the particles ten times stiffer than the matrix and for the volume fraction of 0.2. Recently, Böhm and Rasool (2016) extended the approach by considering elasto-plastic behavior of the matrix material. In addition to the contribution tensors of individual pores, Drach et al. (2016) used FEA to study the shape effects of cubical, octahedral and tetrahedral pores on the overall elastic properties of porous materials using periodic RVEs containing parallel and randomly oriented pores.

The inverse problem – design of microstructures of particle-reinforced composites – has been studied extensively in the works of Zohdi (2001), Zohdi (2003a), Zohdi (2003b). The author presents efficient computational algorithms for determining volume fractions, shapes, mechanical properties and orientations of particles for doping of a homogeneous matrix material so that the overall composite properties match the desired. The methodology is based on "microstructure-nonconforming" FEA approach.

Table 1. Examples of ipolyhedral shapes

Shape	Idealized	Microscopy	Shape	Idealized	Microscopy
Sphere [1]	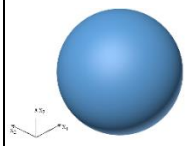	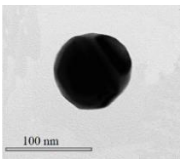	Truncated Octahedron [6]	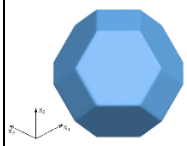	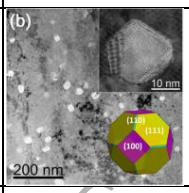
Polyhedral Supersphere (smooth) [2]	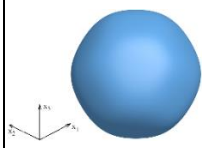	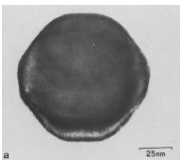	Cuboctahedron [7]	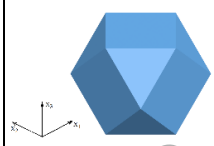	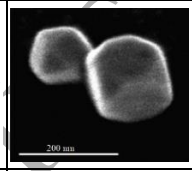
Polyhedral Supersphere (smooth) [2]	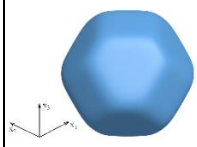	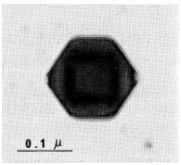	Rhombic Dodecahedron [8]	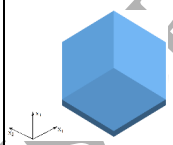	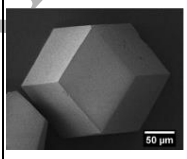
Cube (smooth) [3]	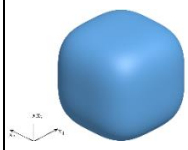	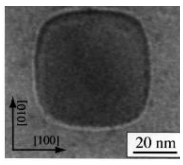	Octahederon (smooth) [7]	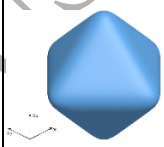	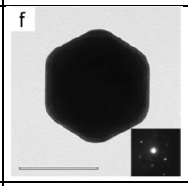
Cube [4]	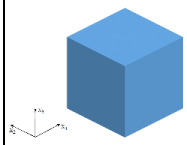	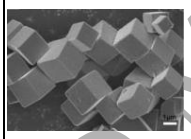	Octahederon [9]	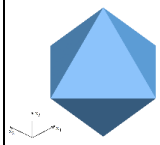	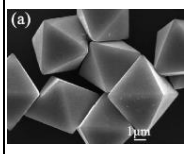
Icosahedron [5]	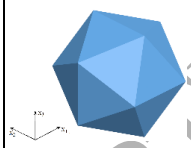	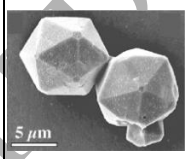	Tetrahedron [10]	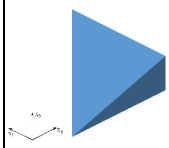	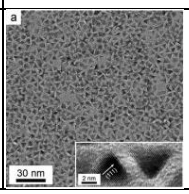

[1] Seo et al. (2006)
[2] Menon and Martin (1986)
[3] Onaka et al. (2003)
[4] Cao et al. (2010)
[5] McMillan (2003)
[6] Zeon Han et al. (2015)
[7] Seo et al. (2006)
[8] Cravillon et al. (2012)
[9] Sun and Yang (2014)
[10] Park et al. (2007)

The shapes in Table 1 can be described using the following general formula combining different types of polyhedra (Onaka (2006), Miyazawa et al. (2012), Onaka (2016)):

$$\left[A_1 h_{hexa} + \frac{A_2}{a^p} h_{octa} + \frac{A_3}{b^p} h_{dodeca}\right]^{1/p} + A_4 {h_{icosa}}^{1/p} + A_5 {h_{tetra}}^{1/p} = 1\,, \qquad (1.1)$$

where $A_1, A_2, A_3, A_4, A_5, A_6$ are constants, p is a shape parameter, and h_{hexa}, h_{octa}, h_{dodeca}, h_{icosa} and h_{tetra} are functions that are given below:

$$h_{hexa} = |x|^p + |y|^p + |z|^p,$$
$$h_{octa} = |x+y+z|^p + |-x+y+z|^p + |x-y+z|^p + |x+y-z|^p,$$
$$h_{dodeca} = |x+y|^p + |x-y|^p + |y+z|^p + |y-z|^p + |x+z|^p + |x-z|^p,$$
$$h_{icosa} = |f(\gamma,\gamma,\gamma)|^p + |f(-\gamma,\gamma,\gamma)|^p + |f(\gamma,-\gamma,\gamma)|^p + |f(\gamma,\gamma,-\gamma)|^p + |f(\xi,\eta,0)|^p + |f(\xi,-\eta,0)|^p + |f(0,\xi,\eta)|^p + |f(0,\xi,-\eta)|^p + |f(\eta,0,\xi)|^p + |f(\eta,0,-\xi)|^p,$$
$$h_{tetra} = H(\gamma,\gamma,\gamma) + (1/p)^{(p-2)} H(-\gamma,-\gamma,-\gamma),$$

where

$$f(a,b,c) = |ax+by+cz|^p, \gamma = \frac{1}{\sqrt{3}}, \xi = \sqrt{\frac{3-\sqrt{5}}{6}}, \eta = \sqrt{\frac{3+\sqrt{5}}{6}},$$
$$H(\gamma,\gamma,\gamma) = \{h(\gamma,\gamma,\gamma)\}^p + \{h(\gamma,-\gamma,-\gamma)\}^p + \{h(-\gamma,\gamma,-\gamma)\}^p + \{h(-\gamma,-\gamma,\gamma)\}^p,$$
$$h(a,b,c) = \{|f(a,b,c)| - f(a,b,c)\}/2.$$

Using formula (1.1) we obtained 15 polyhedral shapes that are analyzed in this paper, see Table 2.

In the present work, we utilize stiffness contribution tensor formalism to estimate overall elastic properties of materials with polyhedral inhomogeneities and compare the results with direct finite element simulations of periodic RVEs. The concept of the stiffness contribution tensor is introduced in section 2. The section also details our numerical approach to calculation of stiffness contribution tensors of individual inhomogeneities. In section 3, we present the components of stiffness contribution tensors of all shapes shown in Table 2. In addition, we investigate the applicability of replacement relations to the considered shapes and introduce a parameter correlating the accuracy of the relations with a shape's geometry. Predictions of the effective elastic properties for particle-reinforced materials with randomly oriented polyhedral inhomogeneities based on stiffness contribution tensors are presented in section 4. The predictions obtained using non-interaction, Mori-Tanaka and Maxwell micromechanical homogenization schemes are compared with direct finite element simulations of periodic RVEs. Section 5 presents the conclusions of the paper. Finally, stiffness contribution tensors of the considered polyhedral shapes for two Poisson's ratio values $\nu_0 = 0.2$ and $\nu_0 = 0.4$ of the matrix (in addition to the results for $\nu_0 = 0.3$ presented in section 3) are given in the Appendix A.

Table 2. Considered polyhedral shapes

#	Shape	Image	A_1	A_2	A_3	A_4	A_5	a	b	p
1	Sphere	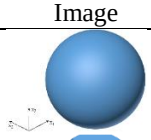	1	0	0	0	0	1	1	2
2	Polyhedral Supersphere 1	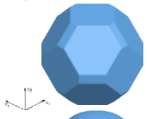	1	1	1	0	0	1.69	1.58	$p \to \infty$
3	Polyhedral Supersphere 1 (smooth)	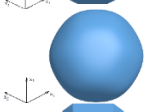	1	1	1	0	0	1.69	1.58	$p = 9$
4	Polyhedral Supersphere 2	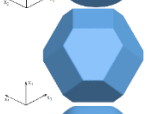	1	1	1	0	0	1.67	1.72	$p \to \infty$
5	Polyhedral Supersphere 2 (smooth)	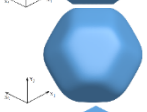	1	1	1	0	0	1.67	1.72	$p = 14.4$
6	Cube	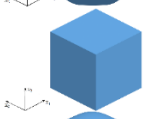	1	0	0	0	0	1	1	$p \to \infty$
7	Cube (smooth)	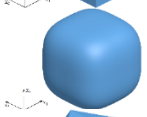	1	0	0	0	0	1	1	$p = 3.3$
8	Icosahedron	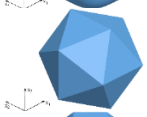	0	0	0	1	0	1	1	$p \to \infty$
9	Truncated Octahedron	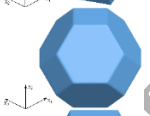	1	1	0	0	0	1.2	1	$p \to \infty$
10	Cuboctahedron	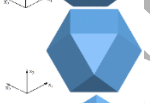	0	1	1	0	0	2	2	$p \to \infty$
11	Rhombic Dodecahedron	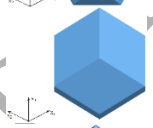	0	0	1	0	0	1	1	$p \to \infty$
12	Octahederon	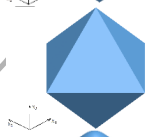	0	1	0	0	0	1	1	$p \to \infty$
13	Octahederon (smooth)	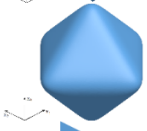	0	1	0	0	0	1	1	$p = 6.44$
14	Tetrahedron	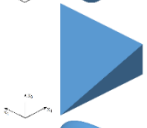	0	0	0	0	1	1	1	$p \to \infty$
15	Tetrahedron (smooth)	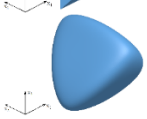	0	0	0	0	1	1	1	$p = 4$

2. Property contribution tensors

Property contribution tensors were first introduced as compliance contribution tensors in the context of pores and cracks by Horii and Nemat-Nasser (1983). Components of such tensors were calculated for 2D pores of various shape and 3D ellipsoidal pores in isotropic material by Kachanov et al. (1994). For the general case of an elastic ellipsoidal inhomogeneity, compliance contribution tensor and its counterpart – stiffness contribution tensor – were presented in Sevostianov and Kachanov (1999, 2002). Kushch and Sevostianov (2015) established the link between these tensors and dipole moments.

Following Sevostianov and Kachanov (1999), we consider a homogeneous isotropic elastic material (matrix) with a stiffness tensor $\mathbf{C}_0$ containing an inhomogeneity of volume V_1 that has a different stiffness $\mathbf{C}_1$. Fourth-rank stiffness contribution tensor $\mathbf{N}$ of an inhomogeneity relates additional stress due to the presence of the inhomogeneity $\boldsymbol{\Delta\sigma}$ (per reference volume V of the elastic material including the inhomogeneity) with applied strain $\boldsymbol{\varepsilon}^0$:

$$\Delta\sigma_{ij} = N_{ijkl}\varepsilon^0_{kl}. \tag{2.1}$$

Strain distribution $\boldsymbol{\varepsilon}$ is assumed to be uniform inside V in the absence of the inhomogeneity. Thus, the stiffness contribution tensor, which characterizes the far-field asymptotic of the elastic fields generated by an inhomogeneity, determines its contribution to the effective elastic properties (Sevostianov and Kachanov, 2011).

We calculate the stiffness contribution tensors (**N**-tensors) of individual particles using FEA. In the procedure, for a given particle geometry we simulate a single inhomogeneity in a large volume subjected to remotely applied uniform displacement fields. To prepare the necessary 3D FEA mesh for the analysis, we begin by generating the surface mesh of the particle in a custom MATLAB script using formula (1.1) and built-in function "isosurface.m". Figure 1 shows the truncated octahedron and icosahedron surface meshes generated using our script. Each mesh is composed of approximately 50,000 elements. The generated surface mesh of a particle is then used in the numerical procedure to find components of the particle property contribution tensor as described below.

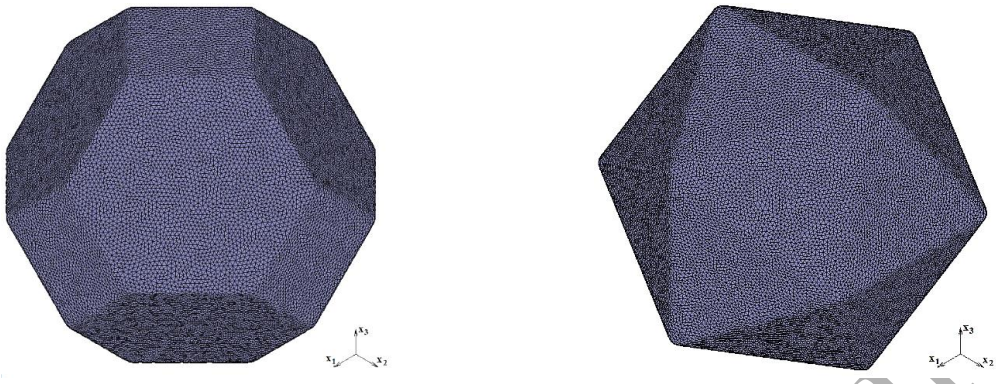

(a) (b)

Figure 1. Particle surface meshes: a) truncated octahedron; b) icosahedron

Particle surface mesh is placed in a large cubic-shaped reference volume with sides five times larger than the largest linear dimension of the particle to reduce boundary effects and simulate remote loading. The setup is auto meshed with 10-node tetrahedral 3D elements (tetra10), see Figure 2. Note, that the choice of the reference volume size and the order of the tetrahedral elements used in the analysis is based on a sensitivity study performed for a particle of spherical shape, for which an analytical solution is available in the literature. In the case of the particle/matrix elastic contrast equal to 20 and 10,000 surface elements used for the particle shape description, the average relative error in FEA calculations of the N-tensor components was calculated to be 0.027%.

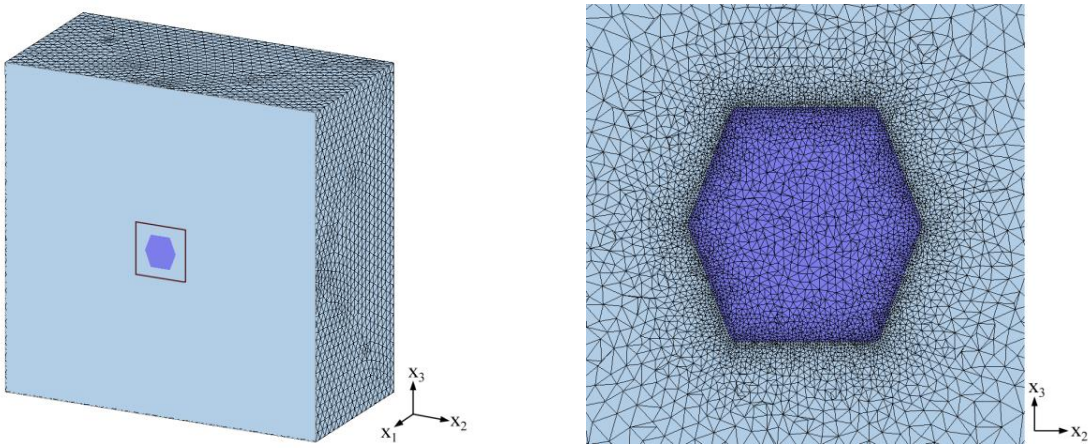

(a) (b)

Figure 2. 3D mesh density of the volume containing an icosahedral particle: a) general view of the reference

volume; b) close-up view of the highlighted region

After volume mesh is generated, the **N**-tensor components are calculated from FEA of six load cases: three uniaxial tension and three shear load cases. All FEA calculations at this stage are performed using commercial multipurpose FEA package MSC Marc Mentat. Boundary conditions for all six load cases are prescribed on the external faces of the reference volume in terms of displacements. Once the six FEA simulations are completed for the given shape, the result files are processed using a custom Python script to determine **N**-tensor. The script starts with calculating volume-averaged stress components within V from each load case:

$$\langle\sigma_{ij}\rangle_m = \frac{1}{V}\sum_{l=1}^{N_e}\left(\sigma_{ij}^{(l)}\right)_m \cdot V^{(l)}, \quad (\mathrm{i,j} = 1,2,3; \quad \mathrm{m} = 1,2,\ldots,6) \tag{2.1}$$

where $\langle\sigma_{ij}\rangle_m$ is the volume average of the stress component ij calculated from the m-th loadcase, V is the reference volume, $\left(\sigma_{ij}^{(l)}\right)_m$ is the stress component ij at the centroid of the finite element l calculated from the m-th loadcase, $V^{(l)}$ is the volume of the element l, and N_e is the total number of elements in the model. Given the average stress components we then calculate the stiffness contribution tensor from:

$$N_{ijkl}(\varepsilon_{kl}^0)_m = \langle\sigma_{ij}\rangle_m - \left(\sigma_{ij}^0\right)_m, \quad \text{(summation over } k,l = 1,2,3) \tag{2.2}$$

where $(\varepsilon_{kl}^0)_m$ are the components of the prescribed strain and $\left(\sigma_{ij}^0\right)_m$ are the stress components inside V in the absence of the inhomogeneity. For example, from the first load case all components N_{ij11} are found (note that all ε_{kl}^0 except ε_{11}^0 are zero):

$$N_{ij11} = \frac{\langle\sigma_{ij}\rangle_1 - \left(\sigma_{ij}^0\right)_1}{\left(\varepsilon_{11}^0\right)_1}. \tag{2.3}$$

Components of the stiffness contribution tensors normalized by particle volume fraction, $\overline{N}_{ijkl} = \left(\frac{V}{V_1}\right)N_{ijkl}$, are presented for different shapes in Table 3.

3. Stiffness contribution tensors of polyhedral particles

3.1. N-tensor components of the considered shapes

Table 3 presents non-zero components of stiffness contribution tensors calculated following the procedure described in section 2 for the shapes presented in Table 2. Young's moduli and Poisson's ratios of the matrix and particle materials used in calculations are $E_0 = 1GPa, \nu_0 = 0.3$, $E_1 = 3GPa, \nu_1 = 0.4$, respectively.

Only three components of the normalized stiffness contribution tensors are presented for the shapes in the first part of Table 3 because the tensors have equal components in three directions: $\bar{N}_{1111}^{FEA} = \bar{N}_{2222}^{FEA} = \bar{N}_{3333}^{FEA}$, $\bar{N}_{1122}^{FEA} = \bar{N}_{2233}^{FEA} = \bar{N}_{3311}^{FEA}$ and $\bar{N}_{1212}^{FEA} = \bar{N}_{2323}^{FEA} = \bar{N}_{3131}^{FEA}$. This means that the tensors are either isotropic or exhibit cubic symmetry. In the case of isotropy, only two out of three presented components are independent and component $\bar{N}_{1212}$ can be expressed as: $\bar{N}_{1212} = (\bar{N}_{1111} - \bar{N}_{1122})/2$. To check the shapes for isotropy, we calculated $\bar{N}_{1212}$ components using the relationship above and compared them with FEA calculations. In the case of a sphere, the relative difference between the isotropic estimate and FEA is 0.0% as expected for a perfectly isotropic shape. Icosahedron can also be considered isotropic with the relative difference of 0.1%. Polyhedral superspheres are close to being isotropic with relative difference values in the range between 0.3 and 0.5%. The rest of the shapes including cube, truncated octahedron, cuboctahedron, rhombic dodecahedron and octahedron have cubic symmetry with cube having the greatest relative difference of 7.4%.

Table 3. Stiffness contribution tensor components of the considered shapes

Shape	$\bar{N}_{1111}^{FEA}$	$\bar{N}_{1122}^{FEA}$	$\bar{N}_{1212}^{FEA}$
Sphere	1.512	0.7701	0.3712
Polyhedral Supersphere 1	1.522	0.7751	0.3746
Polyhedral Supersphere 1 (smooth)	1.513	0.7710	0.3720
Polyhedral Supersphere 2	1.524	0.7769	0.3757
Polyhedral Supersphere 2 (smooth)	1.516	0.7730	0.3733
Cube	1.583	0.7837	0.3719
Cube (smooth)	1.530	0.7685	0.3681
Icosahedron	1.523	0.7745	0.3739
Truncated Octahedron	1.523	0.7803	0.3784
Cuboctahedron	1.539	0.7746	0.3720

Rhombic Dodecahedron	1.524	0.7815	0.3791
Octahedron	1.540	0.7934	0.3850
Octahedron (smooth)	1.522	0.7846	0.3813

Shape	$\bar{N}_{1111}^{FEA}$	$\bar{N}_{1122}^{FEA}$	$\bar{N}_{1212}^{FEA}$	$\bar{N}_{3333}^{FEA}$	$\bar{N}_{1133}^{FEA}$	$\bar{N}_{1313}^{FEA}$
Tetrahedron	1.622	0.8034	0.3698	1.583	0.8427	0.4091
Tetrahedron (smooth)	1.551	0.7780	0.3693	1.534	0.7948	0.3862

3.2. Replacement relations

Replacement relations play an important role in geomechanics in the context of the effect of saturation on seismic properties of rock. This problem was first addressed by Gassmann (1951) who proposed the following relation expressing bulk modulus K of fully saturated rock in terms of the elastic properties of dry rock (see Mavko et al. (2009), Jaeger et al. (2007) for application of these relations in rock mechanics and geophysics):

$$K = K_{dry} + \frac{K_0\left(1-K_{dry}/K_0\right)^2}{1-\varphi-K_{dry}/K_0+\varphi K_0/K_1}, \tag{3.1}$$

where subscripts "0" and "1" denote elastic constants of the matrix material and material filling the pores, respectively; φ is the volume fraction of the inhomogeneities (porosity for the material with unfilled pores); K_{dry} is the bulk modulus of the porous material of the same morphology. This approach was further developed in the works of Ciz and Shapiro (2007) who obtained relation similar to (3.1) for shear modulus and Saxena and Mavko (2014) who derived replacement relations (they use term "substitution relations") for isotropic rocks containing inhomogeneities of the same shape, but different elastic constants. The latter were obtained under the assumption that strains and stresses inside inhomogeneities are uniform and overall properties and properties of the constituents are isotropic. Replacement relations for the most general case were obtained by Sevostianov and Kachanov (2007) in terms of property contribution tensors of inhomogeneities having the same shape but different elastic constants and embedded in the same matrix:

$$\frac{V_1}{V}(\mathbf{N}_A^{-1} - \mathbf{N}_B^{-1}) = (\mathbf{C}_A - \mathbf{C_0})^{-1} - (\mathbf{C}_B - \mathbf{C_0})^{-1} \tag{3.2}$$

where $\mathbf{N}_A$ and $\mathbf{N}_B$ are the stiffness contribution tensors of inhomogeneities with material properties A and B, respectively, $\mathbf{C}_A$ and $\mathbf{C}_B$ are the stiffness tensors of particles having material properties A and B, and $\mathbf{C_0}$ is the stiffness tensor of matrix material. (Chen et al., 2017) showed that these relations lead to the following one relating effective properties of a dry porous material and material containing inhomogeneities with material properties A having the same morphology:

$$\mathbf{S}^{NI} = \mathbf{S}_0 + \varphi\left[(\mathbf{S}_A - \mathbf{S}_0)^{-1} + \varphi\left(\mathbf{S}_{dry} - \mathbf{S}_0\right)^{-1}\right]^{-1}, \tag{3.3}$$

where **S** denotes compliance tensor of a material.

For an isotropic mixture of inhomogeneities, (3.3) yields the following expressions for effective bulk and shear moduli K and G:

$$K = K_0 \frac{\varphi K_{dry}(K_0 - K_A) + K_A(K_0 - K_{dry})}{\varphi K_0(K_0 - K_A) + K_A(K_0 - K_{dry})},$$

$$G = G_0 \frac{\varphi G_{dry}(G_0 - G_A) + G_A(G_0 - G_{dry})}{\varphi G_0(G_0 - G_A) + G_A(G_0 - G_{dry})}. \tag{3.4}$$

These relations coincide with the ones obtained by Gassmann (1951), Ciz and Shapiro (2007), and Saxena and Mavko (2014). Moreover, relations (3.4) are independent of the homogenization method (e.g. non-interaction approximation, Mori-Tanaka scheme, Maxwell scheme etc.) provided that properties of both porous material and the composite are calculated using the same method. (Chen et al., 2017) also showed that replacement relations (3.2) and (3.3), being exact for inhomogeneities of ellipsoidal shape, can be used as an accurate approximation for non-ellipsoidal convex superspheres. In this section, we investigate the applicability of the replacement relation (3.2) to the polyhedral shapes presented in Table 2.

We start with an inhomogeneity A having elastic properties $E_A = 3GPa,\ \nu_A = 0.4$ (see Table 3) and calculate the stiffness contribution tensor for inhomogeneity B of the same shape having elastic properties $E_B = 20GPa,\ \nu_B = 0.2$ using the replacement relation (3.2). Matrix material is the same in both cases with Young's modulus and Poisson's ratio equal to $E_0 = 1GPa$ and $\nu_0 = 0.3$, respectively. Table 4 presents the comparison between stiffness contribution tensors calculated via FEA ($\bar{N}_{ijkl}^{FEA}$) and obtained utilizing the replacement relation ($\bar{N}_{ijkl}^{repl.}$) as

described above for all shapes presented in Table 2. The table also contains unsigned relative errors for individual components ($\Delta\bar{N}_{ijkl}$) and Euclidean norm of the absolute error ($\|\mathbf{N}^{FEA} - \mathbf{N}^{repl.}\|$). Additional results for $\nu_0 = 0.2$ and $\nu_0 = 0.4$ are presented in Appendix A.

Table 4. Comparison between stiffness contribution tensors calculated via direct FEA and obtained utilizing the replacement relation. Matrix material: $E_0 = 1GPa$ and $\nu_0 = 0.3$, particle material: $E_1 = 20GPa$, $\nu_1 = 0.2$

Shape	$\bar{N}_{1111}^{FEA}$	$\bar{N}_{1122}^{FEA}$	$\bar{N}_{1212}^{FEA}$	$\bar{N}_{1111}^{repl.}$	$\bar{N}_{1122}^{repl.}$	$\bar{N}_{1212}^{repl.}$	$\Delta\bar{N}_{1111}$ (%)	$\Delta\bar{N}_{1122}$ (%)	$\Delta\bar{N}_{1212}$ (%)	$\|\mathbf{N}^{FEA} - \mathbf{N}^{repl.}\|$
Sphere	2.169	0.7014	0.7331	2.169	0.7014	0.7331	0.00	0.00	0.00	0.000
Polyhedral Supersphere 1 (smooth)	2.168	0.7035	0.7372	2.174	0.7050	0.7416	0.08	0.01	0.11	0.009
Polyhedral Supersphere 1	2.210	0.7036	0.7571	2.188	0.7050	0.7468	1.03	0.20	1.35	0.024
Polyhedral Supersphere 2 (smooth)	2.185	0.7044	0.7465	2.174	0.7050	0.7416	0.50	0.08	0.65	0.012
Polyhedral Supersphere 2	2.224	0.7047	0.7659	2.193	0.7065	0.7512	1.38	0.26	1.92	0.033
Cube (smooth)	2.240	0.6835	0.7304	2.226	0.6824	0.7214	0.50	0.16	1.24	0.016
Cube	2.505	0.6617	0.7932	2.372	0.6667	0.7361	5.29	0.75	7.20	0.137
Icosahedron	2.216	0.7013	0.7564	2.193	0.7025	0.7439	1.07	0.17	1.65	0.025
Truncated Octahedron	2.213	0.7168	0.7816	2.183	0.7154	0.7618	1.34	0.19	2.52	0.033
Cuboctahedron	2.291	0.6849	0.7559	2.244	0.6882	0.7365	2.02	0.48	2.56	0.050
Rhombic Dodecahedron	2.218	0.7194	0.7901	2.184	0.7172	0.7646	1.54	0.31	3.23	0.039
Octahedron (smooth)	2.204	0.7344	0.8099	2.172	0.7258	0.7736	1.45	1.17	4.48	0.049
Octahedron	2.282	0.7472	0.8617	2.214	0.7298	0.7892	2.97	2.33	8.42	0.103

Shape	Tetrahedron (smooth)	Tetrahedron
$\bar{N}_{1111}^{FEA}$	2.339	2.754

$\bar{N}_{1122}^{FEA}$	0.6937	0.7024
$\bar{N}_{1212}^{FEA}$	0.7911	0.9141
$\bar{N}_{3333}^{FEA}$	2.310	2.644
$\bar{N}_{1133}^{FEA}$	0.7232	0.8128
$\bar{N}_{1313}^{FEA}$	0.8205	1.0241
$\bar{N}_{1111}^{repl.}$	2.262	2.432
$\bar{N}_{1122}^{repl.}$	0.6695	0.6339
$\bar{N}_{1212}^{repl.}$	0.7260	0.7280
$\bar{N}_{3333}^{repl.}$	2.194	2.262
$\bar{N}_{1133}^{repl.}$	0.7379	0.8040
$\bar{N}_{1313}^{repl.}$	0.7941	0.8977
$\max(\Delta\bar{N}_{ijkl}(\%))$	8.22	20.35
$\|\mathbf{N}^{FEA} - \mathbf{N}^{repl.}\|$	0.131	0.400

Sphere is a special case of an ellipsoid for which the replacement relation is exact. Therefore, there should be no difference between FEA results and **N**-tensor values obtained via replacement relation in the case of a sphere. As expected relative errors as well as Euclidean norm of the absolute error are zero, see the first row in Table 3. Calculations for other shapes result in non-zero relative errors and error norms with the largest relative error and error norm observed in the case of a tetrahedron. Based on Table 3, it can be concluded that the replacement relation can be applied to most of the considered shapes with very good accuracy (maximum error <5%) except for a cube, octahedron, tetrahedron and a smooth tetrahedron for which the maximum relative errors are higher – 7.2%, 8.4%, 20.4% and 8.2%, respectively. Note that the replacement relation works better for shapes with low values of the parameter p, which has the effect of smoothing of the edges and corners of a shape.

It appears that the errors in the replacement relation predictions are smaller for the shapes resembling a sphere (e.g. smooth polyhedral superspheres) and greater for the shapes different from the sphere (e.g. cube, tetrahedron). The parameter that can be used to measure the "sphericity" of a shape is the ratio $S^{3/2}/V$, where S is the surface area and V is the volume of the

shape. Among all possible 3D shapes, a sphere has the minimum surface area for a given volume and the ratio $S^{3/2}/V = 10.63$. Figure 3a presents the Euclidean norm of the absolute error in replacement relation results for different shapes as a function of the surface area-to-volume parameter. Figure 3b presents the Euclidean norm of the absolute difference between the FEA calculated **N**-tensors of different shapes and **N**-tensor of a sphere. Two conclusions can be drawn from the figures: a) the error norm increases linearly with the parameter $S^{3/2}/V$; and b) the error norms in Figure 3b are almost half of the error norms in Figure 3a for the corresponding shapes. The latter conclusion indicates that the replacement relation (3.2) results in a better N-tensor approximation for a given inhomogeneity shape and elastic properties combination compared to a simple replacement of the shape with a sphere.

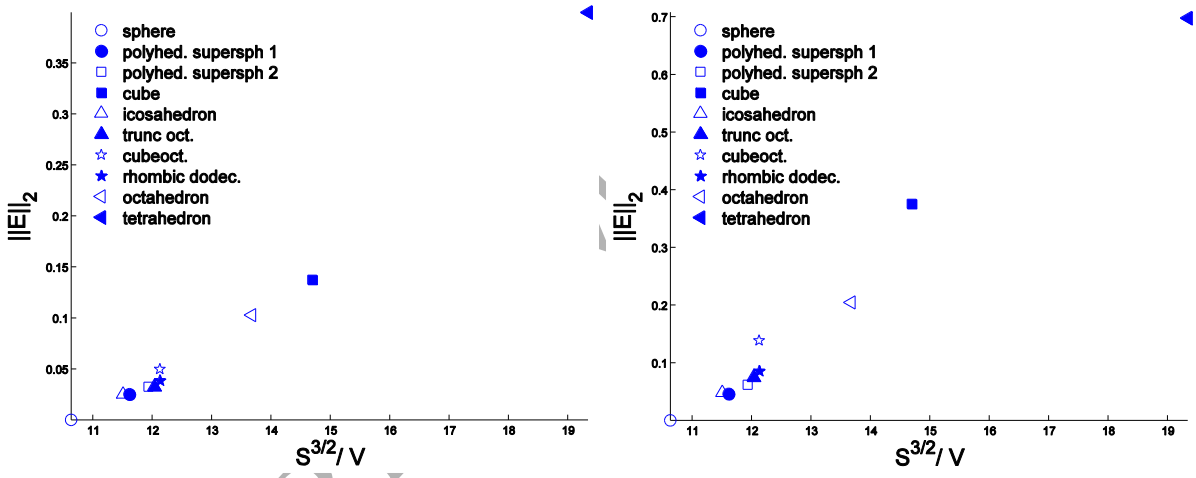

Figure 3. Effect of the surface area-to-volume ratio parameter of a shape on the Euclidean norm of the absolute error: (a) between N-tensors of the polyhderal shapes from Table 2 calculated via FEA and replacement relation; (b) between N-tensors of the polyhedral shapes from Table 2 calculated via FEA and N-tensor of a sphere

4. Effective elastic properties

In this section, we use N-tensors of individual shapes to estimate effective elastic moduli of materials containing randomly oriented inhomogeneities of the same shape. We focus on five shapes – polyhedral supersphere 1, rhombic dodecahedron, icosahedron, cuboctahedron and octahedron.

4.1. Analytical homogenization based on N-tensor

To characterize contribution of multiple particles to the effective elastic properties a homogenization procedure based on **N**-tensor is used. The effective stiffness tensor of a material with particles is given by

$$\mathbf{C} = \mathbf{C_0} + \Delta\mathbf{C}_{\mathrm{RVE}} \tag{4.1}$$

where $\mathbf{C_0}$ is the stiffness tensor of the matrix material and $\Delta\mathbf{C}_{\mathrm{RVE}}$ is the collective contribution of all particles to the overall stiffness of the representative volume element.

The non-interaction scheme provides a reasonably good approximation for a dilute distribution of particles, and $\Delta\mathbf{C}_{\mathrm{RVE}}$ in this case is obtained by direct summation of contributions from all individual particles in the RVE:

$$\Delta\mathbf{C}^{\mathrm{NI}}_{\mathrm{RVE}} = \sum_{\mathrm{i}} \mathbf{N}_{(\mathrm{i})}, \tag{4.2}$$

where $\mathbf{N}_{(i)}$ is the stiffness contribution tensor of the *i*-th particle. The procedure for calculation of stiffness contribution tensors of individual particles is presented in section 2.

For higher volume fractions when interaction between particles is significant and the non-interaction approximation is no longer applicable, more advanced micromechanical schemes should be used. One of the most widely used is the Mori-Tanaka scheme, proposed in Mori and Tanaka (1973) and clarified in Benveniste (1987). Following this approximation the combined contribution of all particles to the overall stiffness of the RVE is given by

$$\Delta\mathbf{C}^{\mathrm{MT}}_{\mathrm{RVE}} = \Delta\mathbf{C}^{\mathrm{NI}}_{\mathrm{RVE}} : \left[\varphi(\mathbf{C_1} - \mathbf{C_0}) + \Delta\mathbf{C}^{\mathrm{NI}}_{\mathrm{RVE}}\right]^{-\mathbf{1}} : (\mathbf{C_1} - \mathbf{C_0}) \tag{4.3}$$

where φ is the volume fraction of particles and $\mathbf{C_1}$ is the stiffness tensor of the inhomogeneity material.

Alternatively, $\Delta\mathbf{C}_{\mathrm{RVE}}$ may be found using Maxwell's homogenization scheme (Maxwell (1873), McCartney and Kelly (2008), Sevostianov (2014)):

$$\Delta\mathbf{C}^{\mathrm{Maxwell}}_{\mathrm{RVE}} = \left\{\left[\Delta\mathbf{C}^{\mathrm{NI}}_{\mathrm{RVE}}\right]^{-1} - \mathbf{P}_{\Omega}\right\}^{-1} \tag{4.4}$$

where $\mathbf{P}_{\Omega}$ is the Hill's tensor (Hill (1965), Walpole (1969)) for the "effective inclusion" of shape Ω. In our study we consider randomly oriented inhomogeneities and therefore the effective inclusion is of spherical shape.

In the framework of non-interaction approximation, contributions from randomly oriented particles of the same shape to the effective bulk and shear moduli can be calculated using the relationship presented in Wu (1966):

$$\frac{K}{K_0} = 1 + \varphi\widetilde{K}\frac{K_0 - K_1}{K_0}, \quad \frac{G}{G_0} = 1 + \varphi\,\widetilde{G}\frac{G_0 - G_1}{G_0}, \tag{4.5}$$

$$\widetilde{K} = \frac{T_{iijj}}{3}, \quad \widetilde{G} = \frac{3T_{ijij} - T_{iijj}}{15} \quad \text{(summation over } i,j = 1,2,3\text{)}, \tag{4.6}$$

where K_o and G_o are bulk and shear moduli of the matrix material, K_1 and G_1 are bulk and shear moduli of the inhomogeneity material, $\mathbf{T}$ is the Wu's strain concentration tensor related to $\mathbf{N}$-tensor and stiffness tensors $\mathbf{C_0}$ and $\mathbf{C_1}$ as $\mathbf{T} = (\mathbf{C_1} - \mathbf{C_0})^{-1}\!:\mathbf{N}$ (Sevostianov and Kachanov (2007)).

Relations for the effective bulk and shear moduli following Mori-Tanaka scheme can be expressed as (see Benveniste (1987)):

$$\frac{K}{K_0} = 1 + \varphi\widetilde{K}\frac{K_1 - K_0}{K_0[(1-\varphi)+\varphi\widetilde{K}]}, \quad \frac{G}{G_0} = 1 + \varphi\widetilde{G}\frac{G_1 - G_0}{G_0[(1-\varphi)+\varphi\widetilde{G}]}, \tag{4.7}$$

Finally, for the Maxwell scheme we have:

$$\frac{K}{K_0} = \frac{E}{3K_0(1-2\nu)}, \quad \frac{G}{G_0} = \frac{E}{2G_0(1+\nu)}, \tag{4.8}$$

where E and ν are the effective Young's modulus and Poisson's ratio that can be calculated from the effective stiffness tensor components, see (4.1).

4.2. Finite element analysis of periodic representative volume elements

The analytical homogenization predictions are compared with direct FEA of RVEs containing multiple inhomogeneities (also known as numerical experiments, see Zohdi and Wriggers (2005)). To generate the RVEs with non-intersecting particles we use a simplified implementation of the collective rearrangement method based on Altendorf and Jeulin (2011) and detailed in Drach et al. (2016). The procedure is implemented in a custom script that results in periodic surface meshes of non-intersecting particles. The RVE surface mesh is imported into MSC Marc/Mentat for further numerical analysis using the "microstructure-conforming" FEA approach (Zohdi and Wriggers (2005)). All FEA model preparation steps at this stage are performed automatically using a custom script that provides a ready-to-run model upon

completion. The final RVE is meshed with 10-node tetrahedral 3D elements. Figure 4 illustrates two examples of generated microstructures.

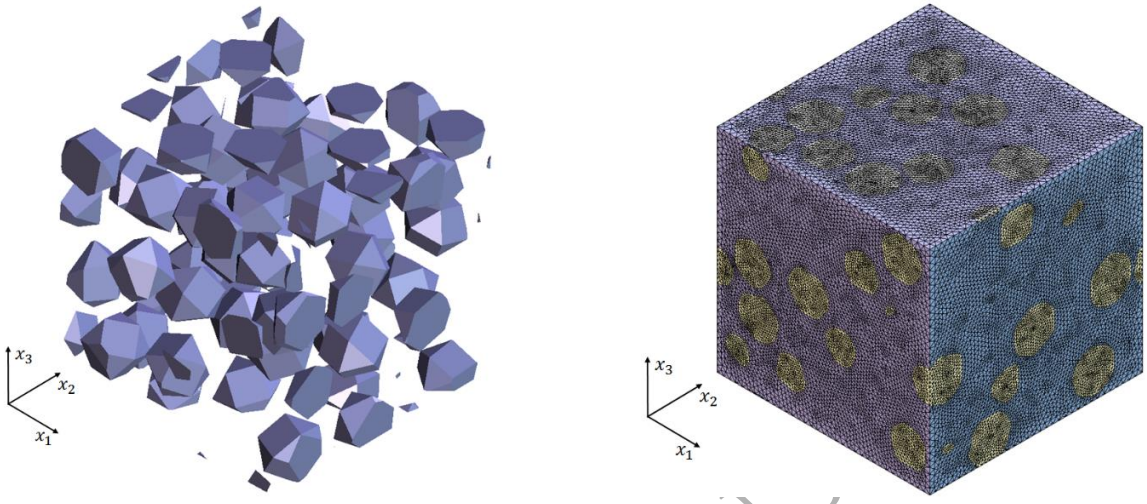

(a) (b)

Figure 4. Illustration of generated RVEs: (a) packed cuboctahedral particles, volume fraction $\varphi = 0.2$: (b) final RVE with polyhedral particles, volume fraction $\varphi = 0.2$

Since RVEs are generated to have congruent meshes on the opposite faces we treat them as unit cells and subject them to periodic boundary conditions. The boundary conditions for two corresponding nodes on the opposite (positive and negative) faces are introduced similarly to Segurado and Llorca (2002):

$$u_j^{(i+)} = u_j^{(i-)} + \delta_j, \quad (j = 1,2,3) \tag{4.9}$$

where $u_j^{(i+)}$ and $u_j^{(i-)}$ are displacements in x_j direction of the *i*-th node on the positive and negative faces respectively; and δ_j is the prescribed average displacement in the x_j direction. Periodic boundary conditions were implemented in MSC Marc/Mentat using the "servo-link" feature (see, for example, Drach et al. (2014), MSC Software (2012), Drach et al. (2016)). Servo-links allow to prescribe multi-point boundary conditions for nodal displacements in the form of a linear function with constant coefficients. In this formulation, δ_j-s are implemented as translational degrees of freedom of control nodes, which are linked to the nodes on the corresponding opposite faces of an RVE. To constrain rigid body displacements, a node inside the RVE is fixed. Rigid body rotations are not allowed by the periodic boundary conditions, so additional constraints are not required.

Six sets of boundary conditions are applied in terms of displacements to simulate three uniaxial tension and three shear load cases. Note that the prescribed strains are set to 0.001 to ensure small deformations so that the initial element volumes could be used in the volume averaging procedure described below. Figure 5a and 5b present stress distributions within two RVE subjected to uniaxial tension along x_1 direction. Once the numerical simulations are performed, the result files are processed using a custom Python script to calculate effective elastic properties of the RVE. First, volume-averaged stress components are calculated for each load case. Given the averaged stress components and applied strain, we calculate the effective stiffness tensor using Hooke's law:

$$C_{ijkl}^{eff}(\varepsilon_{kl}^{0})_m = \langle\sigma_{ij}\rangle_m, \tag{4.10}$$

where $\langle\sigma_{ij}\rangle_m$ and $(\varepsilon_{kl}^{0})_m$ are the volume-averaged stress and applied strain components, respectively, and m is the load case number. For example, from the second load case we can calculate all C_{ij22}^{eff} components:

$$C_{ij22}^{eff} = \frac{\langle\sigma_{ij}\rangle_2}{(\varepsilon_{22}^{0})_2}. \tag{4.11}$$

Engineering constants are then obtained from the effective compliance tensor assuming orthotropic effective response, in which case the tensor can be expressed in the following matrix form:

$$\boldsymbol{S}^{eff} = \begin{bmatrix} \frac{1}{E_1} & -\frac{\nu_{21}}{E_2} & -\frac{\nu_{31}}{E_3} & 0 & 0 & 0 \\ -\frac{\nu_{12}}{E_1} & \frac{1}{E_2} & -\frac{\nu_{32}}{E_3} & 0 & 0 & 0 \\ -\frac{\nu_{13}}{E_1} & -\frac{\nu_{23}}{E_2} & \frac{1}{E_3} & 0 & 0 & 0 \\ 0 & 0 & 0 & \frac{1}{2G_{23}} & 0 & 0 \\ 0 & 0 & 0 & 0 & \frac{1}{2G_{31}} & 0 \\ 0 & 0 & 0 & 0 & 0 & \frac{1}{2G_{12}} \end{bmatrix}. \tag{4.12}$$

The overall isotropic Young's modulus and Poisson's ratio are calculated as averages of E_1, E_2, E_3 and ν_{12}, ν_{23}, ν_{31}, respectively. The average relative error between the moduli E_1, E_2 and E_3 was observed to be below 0.1%.

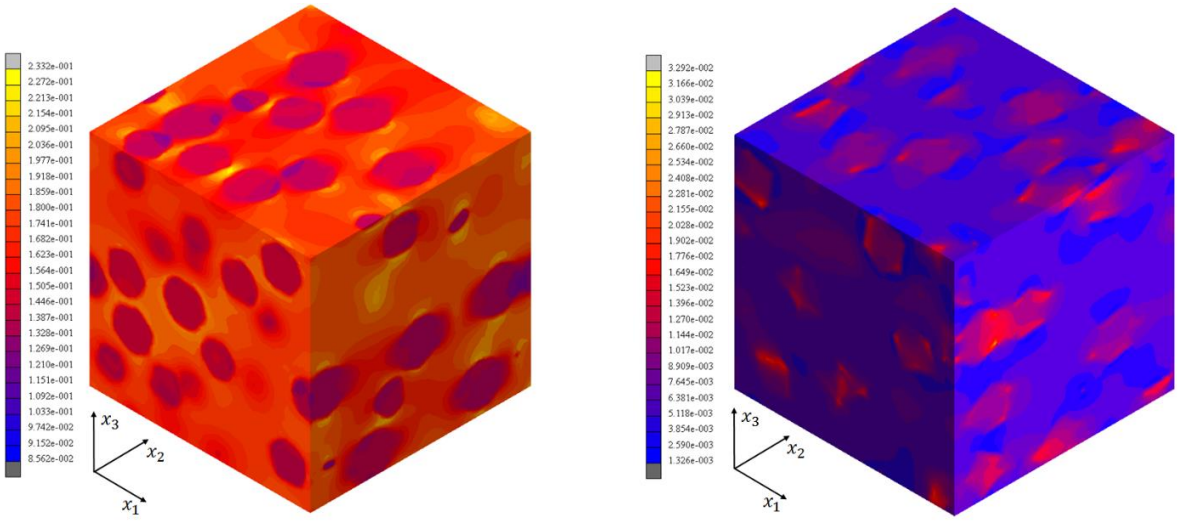

(a) (b)

Figure 5. Distribution of σ_{11} stress component (GPa) within an RVE subjected to uniaxial tension along x_1 direction: (a) matrix material with $E_0 = 120\ GPa$ and $\nu_0 = 0.34$, polyhedral supersphere particles with $E_1 = 70\ GPa$ and $\nu_1 = 0.35$, volume fraction $\varphi = 0.2$; (b) matrix material with $E_0 = 2.89\ GPa$ and $\nu_0 = 0.35$, cuboctahedral particles with $E_1 = 79\ GPa$ and $\nu_1 = 0.4$, volume fraction $\varphi = 0.2$

4.3. Results

Effective bulk (K) and shear (G) moduli of materials containing five types of particles selected from Table 2 (polyhedral supersphere 1, rhombic dodecahedron, icosahedron, cuboctahedron and octahedron) were approximated using non-interaction, Mori-Tanaka and Maxwell homogenization schemes based on numerically calculated **N**-tensors for individual particles. Table 5 presents elastic properties of the matrix and inhomogeneity materials that were used in homogenization. The results are compared to FEA simulations performed on RVEs containing 50 particles each (see section 6.5.1 in Zohdi and Wriggers (2005) for discussion on sufficient number of particles) with volume fractions $\varphi = 0.10, 0.15, 0.20$ for the octahedral shape and $\varphi = 0.10, 0.20, 0.30$ for all other shapes. For each microstructure five RVE realizations were generated. Each realization is shown as a separate data point. All results are presented in Figure 6.

Good correspondence between FEA simulations and Mori-Tanaka and Maxwell schemes is observed with the latter being a little closer to the direct FEA, see Figures 6a-e. From Figure 6a it can be concluded that Maxwell and Mori-Tanaka schemes produce almost identical predictions, since polyhedral supersphere 1 is very close to the spherical shape for which Maxwell and Mori-

Tanka schemes coincide. Note that with increasing elastic contrast between the matrix and the particles, correlation between homogenization schemes and direct FEA decreases. The greatest elastic contrast considered in this paper (~360) was used for the material with octahedral particles (Figure 6e). The maximum relative error between the Maxwell scheme and direct FEA in this case is observed in shear modulus predictions and is equal to 2.5%.

Table 5. Elastic properties of the considered material combinations

Particle shape	**Matrix material**		**Particle material**	
	E_0, GPa	ν_0	E_1, GPa	ν_1
polyhedral supersphere 1	120	0.34	70	0.35
rhombic dodecahedron	70	0.17	3.5	0.44
icosahedron	2.5	0.34	83	0.37
cuboctahedron	2.89	0.35	79	0.4
octahedron	2.89	0.35	1050	0.1

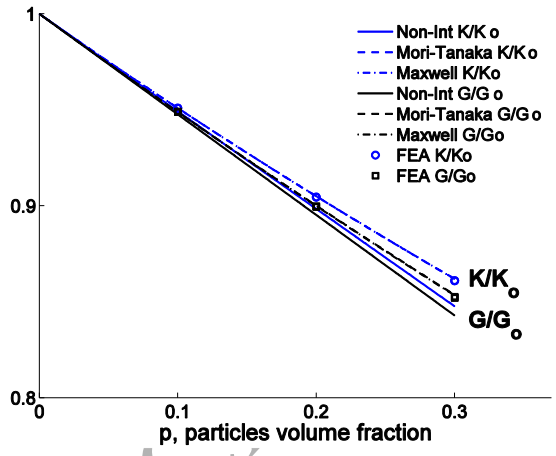

(a)

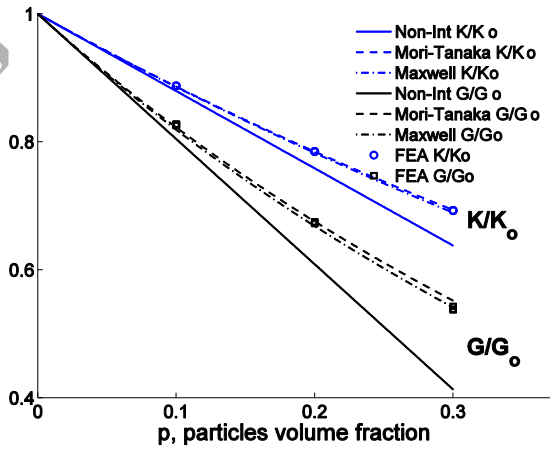

(b)

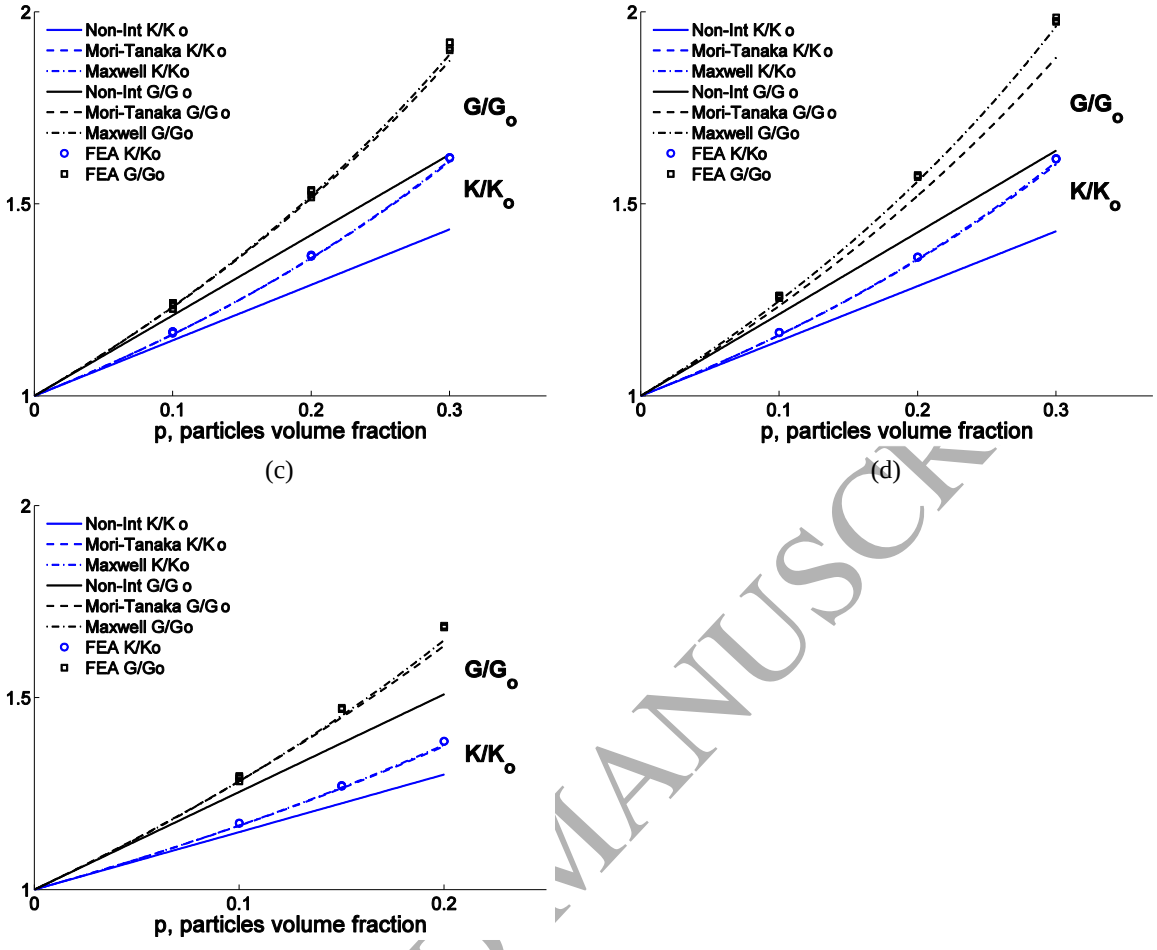

Figure 6. Effective elastic properties of materials containing randomly oriented particles of different shapes: a) polyhedral supersphere 1 (smooth); b) rhombic dodecahedron; c) icosahedron; d) cuboctahedron; e) octahedron

The replacement relation (3.2) interrelates contributions of inhomogeneities having the same shape but different elastic constants to the overall elastic properties. This allows extending the results presented in section 3.1 and Appendix A to combinations of matrix/particle properties not discussed in the paper. Here we investigate the accuracy of K and G predictions based on the replacement relation for materials containing randomly oriented octahedral, cubical, and tetrahedral particles. The predictions were obtained using Maxwell homogenization scheme based on N-tensors of polyhedral particles estimated using the relation (3.2). First, we obtained N-tensor components of the individual shapes for $E_0 = 1, \nu_0 = 0.33, E_1 = 20$ and $\nu_1 = 0.2$ by interpolating the components for $\nu_0 = 0.3$ and $\nu_0 = 0.4$ presented in Table 4 and Appendix A, respectively. Then, we applied the replacement relation (3.2) to estimate the N-tensor

components for $E_0 = 1, \nu_0 = 0.33, E_1 = 10$ and $\nu_1 = 0.1$, and used the result to predict effective bulk and shear moduli for $\varphi = 0.2$. The predictions are compared to the FEA results for periodic RVEs published in Rasool and Böhm (2012) and presented in Table 6. Note that the moduli K_{RB} were calculated based on the effective Young's moduli and Poisson's ratios from Table 3 in Rasool and Böhm (2012) because we believe the authors made a mistake in their calculations of the effective bulk moduli in the paper.

From the analysis of Table 6 we conclude that Maxwell scheme in combination with the replacement relation (3.2) provide very good estimates for the effective bulk moduli of all three shapes (relative error <1%) and good predictions for the effective shear moduli except for a cube (relative error of 6.14%).

Table 6. Comparison of effective bulk and shear moduli predictions for materials containing randomly oriented particles of octahedral, cubical and tetrahedral shapes ($\varphi = 0.2$) based on the replacement relation (3.2) with numerical calculations presented in Rasool and Böhm (2012)

Particle shape	**Rasool and Böhm (2012)**		**Our predictions**		**Unsigned rel. error, %**	
	K_{RB}	G_{RB}	K	G	$\Delta K\%$	$\Delta G\%$
Octahedron	1.248	1.479	1.254	1.450	0.51	1.93
Cube	1.263	1.466	1.257	1.562	0.45	6.14
Tetrahedron	1.271	1.529	1.280	1.590	0.75	3.82

In addition, we looked at the performance of the replacement relation in two extreme cases – when **N**-tensors of elastic particles are estimated from **N**-tensors of pores and from N-tensors of perfectly rigid particles. We began by calculating **N**-tensors for pores ($E_1 = 0$) and perfectly rigid inhomogeneities ($E_1 \to \infty$) for the five shapes discussed above (polyhedral supersphere 1, rhombic dodecahedron, icosahedron, cuboctahedron and octahedron), then used the results to calculate **N**-tensors for elastic properties from Table 5 via the replacement relation. Stiffness contribution tensor components for the five particles having $E_1 = 0\ GPa$ and $E_1 = 10^6\ GPa$ are presented in Table 7. Finally, we estimated the effective bulk (K) and shear (G) moduli using Maxwell homogenization scheme. The results are compared with direct FEA simulations and effective elastic properties of RVEs containing spheres, and presented in Figure 7.

Table 7. Stiffness contribution tensor components for pores and rigid particles of the following shapes: polyhedral supersphere 1, rhombic dodecahedron, icosahedron, cuboctahedron and octahedron

Shape	Rigid, $E_1 = 10^6\ GPa$			Pore, $E_1 = 0\ GPa$		
	$\bar{N}_{1111}^{rigid}$	$\bar{N}_{1212}^{rigid}$	$\bar{N}_{1122}^{rigid}$	$\bar{N}_{1111}^{pore}$	$\bar{N}_{1212}^{pore}$	$\bar{N}_{1122}^{pore}$
polyhedral supersphere1, $E_0 = 120\ GPa, \nu_0 = 0.34$	315.4	98.33	120.7	-508.6	-84.27	-337.9
rhombic dodecahedron, $E_0 = 70\ GPa, \nu_0 = 0.17$	160.3	65.07	37.22	-157.9	-62.72	-28.17
icosahedron, $E_0 = 2.5\ GPa, \nu_0 = 0.34$	6.727	2.103	2.504	-10.77	-1.786	-7.207
cuboctahedron, $E_0 = 2.89\ GPa, \nu_0 = 0.35$	8.285	2.428	3.007	-13.99	-2.158	-10.05
octahedron, $E_0 = 2.89\ GPa, \nu_0 = 0.35$	8.177	3.292	2.977	-15.18	-2.326	-10.82

From the examination of the Figures 7a and 7b it can be concluded that in the case of soft inhomogeneities, Maxwell scheme in combination with **N**-tensor obtained from the replacement relation based on a pore provides a good correlation with direct FEA results. On the other hand, for stiff inhomogeneities, Maxwell scheme predictions with **N**-tensor obtained from the replacement relation based on a perfectly rigid particle result in a better agreement with direct FEA calculations, see Figures 7c-e. Comparing the predictions for the effective moduli from spheres with direct FEA results indicates that the effective shear modulus is more sensitive to the shape of inhomogeneitis than the effective bulk modulus. In addition, the results show that predictions obtained from the replacement relation work better than approximations by spheres.

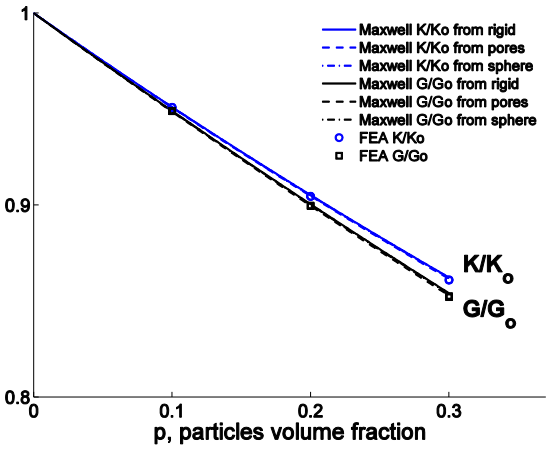

(a)

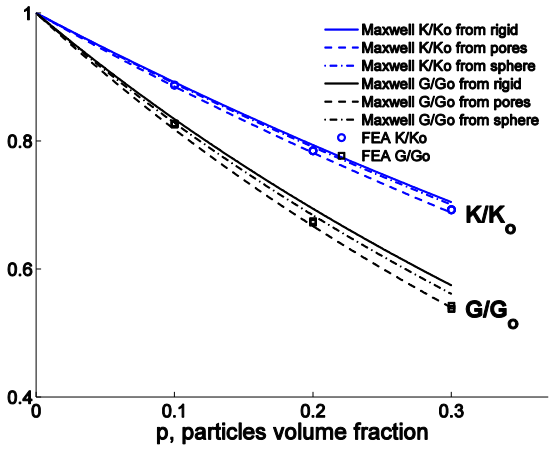

(b)

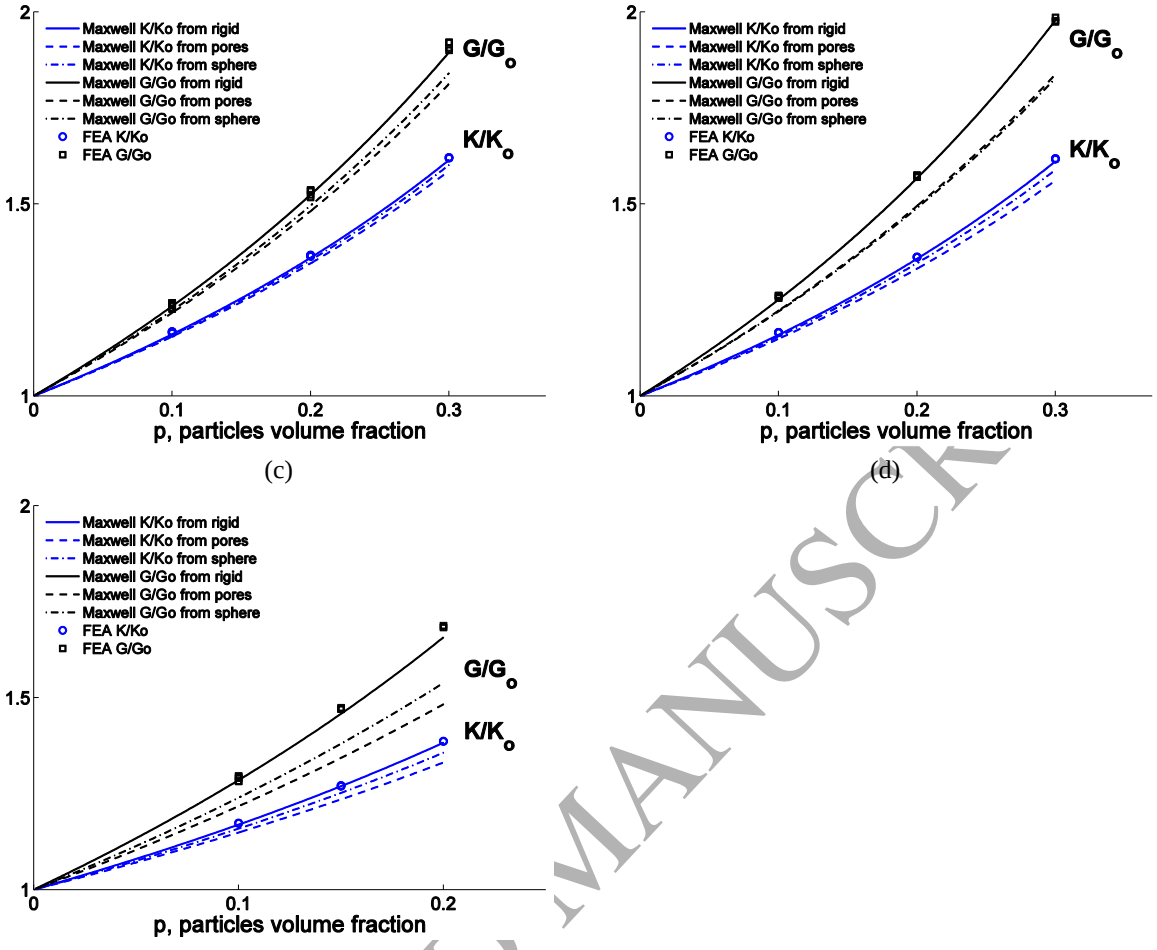

Figure 7. Effective elastic properties estimated via Maxwell scheme and N-tensors based on the replacement relation of materials containing randomly oriented particles of different shapes: a) polyhedral supersphere1; b) rhombic dodecahedron; c) icosahedron; d) cuboctahedron; e) octahedron

5. Conclusions

Stiffness contribution tensors (N-tensors) of 15 convex polyhedra were calculated using Finite Element Analysis and presented in this paper. The N-tensor components of these shapes were analyzed to determine whether the tensors were isotropic or exhibited cubic symmetry. As expected, a sphere was confirmed to be isotropic; polyhedral superspheres were found to be nearly isotropic; and a cube, truncated octahedron, cuboctahedron, rhombic dodecahedron and octahedron were concluded to have cubic symmetry.

The applicability of the replacement relation that interrelates stiffness contribution tensors of inhomogeneities having the same shape but different elastic properties to the considered shapes

was investigated. It was found that the replacement relation can be used with good accuracy (<5% maximum relative error) for most of the considered shapes except for a tetrahedron, octahedron, cube and smooth tetrahedron for which the maximum relative errors were considerably higher. Application of the replacement relation to a tetrahedron resulted in the largest relative error of 20.4% among all considered shapes. Note that the replacement relation works better for shapes with low values of the parameter p, which has the effect of smoothing of the edges and corners of a shape. We also observed a correlation between the accuracy of the replacement relation and the sphericity shape parameter – the Eucledian norm of the difference between N-tensor calculated via replacement relation and N-tensor obtained from direct FEA increases linearly with sphericity. Similar correlation was observed for the Eucledian norm of the difference between the N-tensor of a polyhedral particle and its approximation by a sphere.

We used N-tensors of individual polyhedra to calculate overall elastic properties of materials containing multiple randomly oriented polyhedral particles via micromechanical homogenization based on non-interaction approximation, Mori-Tanaka and Maxwell schemes. The results were compared with direct FEA calculations performed on periodic RVEs. Good correspondence between FEA simulations and Mori-Tanaka and Maxwell schemes up to volume fractions of 30% was observed with Maxwell scheme being a little closer to direct FEA. FEA results were also compared with effective properties calculated using Maxwell scheme and the replacement relation based on perfectly rigid particles and pores. We observed that in the cases when particle material is stiffer than the matrix, the replacement relation based on perfectly rigid particles results in good predictions for effective elastic properties. Conversely, in the cases when particles are softer than the matrix, the replacement relation based on pores produces better estimates for the overall elastic properties.

Combination of N-tensor components presented in this paper for different values of matrix Poisson's ratio (see Table 4 and Appendix A) with the replacement relation (3.2) can be used to estimate stiffness contribution tensors of polyhedral particles for any set of particle/matrix elastic properties. The estimate will have a particularly good accuracy in the cases when particles are stiffer than the matrix because Table 4 and Appendix A results were obtained for stiff particles. For a combination in which the particle material is softer than the matrix, approximation of the

shape by a sphere might result in a better estimate than the one obtained from the replacement relation based on a stiff particle.

Acknowledgements. Financial support from the New Mexico Space Grant Consortium through NASA Cooperative Agreements NNX13AB19A and NNX15AK41A is gratefully acknowledged.

Appendix A

Table A.1. Comparison between stiffness contribution tensors calculated via direct FEA and obtained utilizing the replacement relation. Matrix material: $E_0 = 1GPa$ and $\nu_0 = 0.2$, particle material: $E_1 = 20GPa$, $\nu_1 = 0.2$

Shape	$\bar{N}_{1111}^{FEA}$	$\bar{N}_{1122}^{FEA}$	$\bar{N}_{1212}^{FEA}$	$\bar{N}_{1111}^{repl.}$	$\bar{N}_{1122}^{repl.}$	$\bar{N}_{1212}^{repl.}$	$\Delta\bar{N}_{1111}$ (%)	$\Delta\bar{N}_{1122}$ (%)	$\Delta\bar{N}_{1212}$ (%)	$\left\|\mathbf{N}^{FEA} - \mathbf{N}^{repl.}\right\|$
Sphere	2.011	0.5026	0.7540	2.011	0.5026	0.7540	0.00	0.00	0.00	0.000
Polyhedral Supersphere 1 (smooth)	2.012	0.5045	0.7576	2.010	0.5046	0.7568	0.10	0.01	0.11	0.002
Polyhedral Supersphere	2.054	0.5057	0.7774	2.031	0.5064	0.7671	1.15	0.13	1.32	0.024
Polyhedral Supersphere 2 (smooth)	2.029	0.5056	0.7669	2.018	0.5059	0.7620	0.56	0.06	0.64	0.012
Polyhedral Supersphere	2.068	0.5069	0.7859	2.037	0.5078	0.7713	1.54	0.19	1.86	0.033
Cube (smooth)	2.078	0.4881	0.7541	2.064	0.4866	0.7449	0.69	0.30	1.23	0.0174
Cube	2.336	0.4771	0.8236	2.201	0.4766	0.7645	5.78	0.10	7.17	0.136
Icosahedron	2.060	0.5038	0.7771	2.035	0.5041	0.7646	1.20	0.07	1.60	0.025
Truncated Octahedron	2.061	0.5172	0.7999	2.030	0.5150	0.7803	1.52	0.43	2.45	0.036
Cuboctahedron	2.129	0.4912	0.7799	2.081	0.4929	0.7601	2.24	0.34	2.54	0.049
Rhombic Dodecahedron	2.068	0.5199	0.8082	2.032	0.5167	0.7831	1.78	0.62	3.11	0.043
Octahedron (smooth)	2.060	0.5327	0.8261	2.024	0.5231	0.7901	1.74	1.80	4.36	0.041
Octahedron	2.146	0.5455	0.8756	2.070	0.5260	0.8046	3.54	3.58	8.11	0.115

Shape	Tetrahedron (smooth)	Tetrahedron
$\bar{N}_{1111}^{FEA}$	2.188	2.623
$\bar{N}_{1122}^{FEA}$	0.4985	0.5155
$\bar{N}_{1212}^{FEA}$	0.8146	0.9411
$\bar{N}_{3333}^{FEA}$	2.160	2.512
$\bar{N}_{1133}^{FEA}$	0.5266	0.6269
$\bar{N}_{1313}^{FEA}$	0.8427	1.052

$\bar{N}_{1111}^{repl.}$	2.106	2.280
$\bar{N}_{1122}^{repl.}$	0.4731	0.4393
$\bar{N}_{1212}^{repl.}$	0.7497	0.7558
$\bar{N}_{3333}^{repl.}$	2.041	2.116
$\bar{N}_{1133}^{repl.}$	0.5381	0.6031
$\bar{N}_{1313}^{repl.}$	0.8145	0.9192
$\max\left(\Delta\bar{N}_{ijkl}(\%)\right)$	7.96	19.69
$\|\mathbf{N}^{FEA} - \mathbf{N}^{repl.}\|$	0.130	0.443

Table A.2. Comparison between stiffness contribution tensors calculated via direct FEA and obtained utilizing the replacement relation. Matrix material: $E_0 = 1GPa$ and $\nu_0 = 0.4$, particle material: $E_1 = 20GPa$, $\nu_1 = 0.2$

Shape	$\bar{N}_{1111}^{FEA}$	$\bar{N}_{1122}^{FEA}$	$\bar{N}_{1212}^{FEA}$	$\bar{N}_{1111}^{repl.}$	$\bar{N}_{1122}^{repl.}$	$\bar{N}_{1212}^{repl.}$	$\Delta\bar{N}_{1111}$ (%)	$\Delta\bar{N}_{1122}$ (%)	$\Delta\bar{N}_{1212}$ (%)	$\left\|\mathbf{N}^{FEA} - \mathbf{N}^{repl.}\right\|$
Sphere	2.721	1.260	0.7300	2.721	1.260	0.7300	0.00	0.00	0.00	0.000
Polyhedral Supersphere 1 (smooth)	2.720	1.262	0.7346	2.718	1.263	0.7337	0.07	0.02	0.12	0.002
Polyhedral Supersphere	2.761	1.260	0.7554	2.738	1.263	0.7445	0.82	0.23	1.44	0.026
Polyhedral Supersphere 2 (smooth)	2.736	1.262	0.7445	2.725	1.263	0.7394	0.39	0.10	0.69	0.012
Polyhedral Supersphere	2.773	1.260	0.7651	2.743	1.264	0.7493	1.10	0.30	2.07	0.034
Cube (smooth)	2.800	1.236	0.7228	2.788	1.235	0.7137	0.45	0.02	1.27	0.013
Cube	3.078	1.192	0.7777	2.945	1.207	0.7207	4.32	1.27	7.32	0.148
Icosahedron	2.768	1.257	0.7542	2.744	1.260	0.7410	0.85	0.23	1.75	0.027
Truncated Octahedron	2.756	1.275	0.7838	2.727	1.275	0.7627	1.04	0.03	2.69	0.029
Cuboctahedron	2.851	1.233	0.7490	2.805	1.240	0.7290	1.64	0.53	2.67	0.053
Rhombic Dodecahedron	2.760	1.277	0.7928	2.728	1.277	0.7654	1.17	0.01	3.46	0.033
Octahedron (smooth)	2.736	1.295	0.8155	2.708	1.289	0.7774	1.00	0.51	4.68	0.041
Octahedron	2.802	1.306	0.8725	2.744	1.293	0.7948	2.09	1.00	8.90	0.085

Shape	Tetrahedron (smooth)	Tetrahedron
$\bar{N}_{1111}^{FEA}$	2.883	3.267
$\bar{N}_{1122}^{FEA}$	1.242	1.226
$\bar{N}_{1212}^{FEA}$	0.7848	0.9041
$\bar{N}_{3333}^{FEA}$	2.850	3.152
$\bar{N}_{1133}^{FEA}$	1.275	1.341
$\bar{N}_{1313}^{FEA}$	0.8179	1.018
$\bar{N}_{1111}^{repl.}$	2.811	2.968
$\bar{N}_{1122}^{repl.}$	1.221	1.175
$\bar{N}_{1212}^{repl.}$	0.7173	0.7123
$\bar{N}_{3333}^{repl.}$	2.735	2.785
$\bar{N}_{1133}^{repl.}$	1.296	1.358
$\bar{N}_{1313}^{repl.}$	0.7924	0.8950
$\max\left(\Delta\bar{N}_{ijkl}(\%)\right)$	8.60	21.22
$\|\mathbf{N}^{FEA} - \mathbf{N}^{repl.}\|$	0.136	0.385

References

Altendorf, H., Jeulin, D., 2011. Random-walk-based stochastic modeling of three-dimensional fiber systems. Physical Review E 83, 41804.

Benveniste, Y., 1987. A new approach to the application of Mori-Tanaka's theory in composite materials. Mechanics of Materials 6, 147–157.

Böhm, H.J., Rasool, A., 2016. Effects of particle shape on the thermoelastoplastic behavior of particle reinforced composites. International Journal of Solids and Structures 87, 90–101.

Cao, Y., Fan, J., Bai, L., Hu, P., Yang, G., Yuan, F., Chen, Y., 2010. Formation of cubic Cu mesocrystals by a solvothermal reaction. CrystEngComm 12, 3894.

Chen, F., Sevostianov, I., Giraud, A., Grgic, D., 2017. Accuracy of the replacement relations for materials with non-ellipsoidal inhomogeneities. International Journal of Solids and Structures 104–105, 73–80.

Chen, F., Sevostianov, I., Giraud, A., Grgic, D., 2015. Evaluation of the effective elastic and conductive properties of a material containing concave pores. International Journal of Engineering Science 97, 60–68.

Ciz, R., Shapiro, S.A., 2007. Saturated With a Solid Material. 72.

Cravillon, J., Schröder, C. a., Bux, H., Rothkirch, A., Caro, J., Wiebcke, M., 2012. Formate modulated solvothermal synthesis of ZIF-8 investigated using time-resolved in situ X-ray diffraction and scanning electron microscopy. CrystEngComm 14, 492.

Drach, A., Drach, B., Tsukrov, I., 2014. Processing of fiber architecture data for finite element modeling of 3D woven composites. Advances in Engineering Software 72, 18–27.

Drach, B., Tsukrov, I., Gross, T.S., Dietrich, S., Weidenmann, K., Piat, R., Böhlke, T., 2011. Numerical modeling of carbon/carbon composites with nanotextured matrix and 3D pores of irregular shapes. International Journal of Solids and Structures 48, 2447–2457.

Drach, B., Tsukrov, I., Trofimov, A., 2016. Comparison of full field and single pore approaches to homogenization of linearly elastic materials with pores of regular and irregular shapes. International Journal of Solids and Structures 10.1016/j.ijsolstr.2016.06.023.

Ekneligoda, T.C., Zimmerman, R.W., 2006. Compressibility of two-dimensional pores having n-fold axes of symmetry. Proceedings of the Royal Society A: Mathematical, Physical and Engineering Sciences 462, 1933–1947.

Ekneligoda, T.C., Zimmerman, R.W., 2008. Shear compliance of two-dimensional pores possessing N-fold axis of rotational symmetry. Proceedings of the Royal Society A: Mathematical, Physical and Engineering Sciences 464, 759–775.

Eshelby, J.D., 1961. Elastic inclusions and inhomogeneities. Progress in Solid Mechanics 2, 89–140.

Eshelby, J.D., 1957. The Determination of the Elastic Field of an Ellipsoidal Inclusion, and Related Problems. Proceedings of the Royal Society A: Mathematical, Physical and Engineering Sciences 241, 376–396.

Garboczi, E.J., Douglas, J.F., 2012. Elastic moduli of composites containing a low concentration of complex-shaped particles having a general property contrast with the matrix. Mechanics of Materials 51, 53–65.

Gassmann, F., 1951. Über die Elastizität poröser Medien. Vierteljahrsschrift der Naturforschenden Gesellschaft in Zurich 96, 1–23.

Hill, R., 1965. A self-consistent mechanics of composite materials. Journal of the Mechanics and Physics of Solids 13, 213–222.

Horii, H., Nemat-Nasser, S., 1983. Overall moduli of solids with microcracks: load-induced anisotropy. Journal of the Mechanics and Physics of Solids 31, 155–171.

Jaeger, J., Cook, N., Zimmerman, R., 2007. Fundamentals of Rock Mechanics. Fourth Edition.

Jasiuk, I., Chen, J., Thorpe, M., 1994. Elastic moduli of two dimensional materials with polygonal and elliptical holes. Applied Mechanics Reviews 47, 18–28.

Kachanov, M., Sevostianov, I., 2012. Rice's Internal Variables Formalism and Its Implications for the Elastic and Conductive Properties of Cracked Materials, and for the Attempts to Relate Strength to Stiffness. Journal of Applied Mechanics 79, 31002.

Kachanov, M., Tsukrov, I., Shafiro, B., 1994. Effective moduli of solids with cavities of

various shapes. Applied Mechanics Reviews 47, S151.

Kushch, V.I., Sevostianov, I., 2015. Effective elastic moduli of a particulate composite in terms of the dipole moments and property contribution tensors. International Journal of Solids and Structures 53, 1–11.

Mavko, G., Mukerji, T., Dvorkin, J., 2009. The Rock Physics Handbook: Tools for Seismic Analysis in Porous Media. Cambridge University Press.

Maxwell, J.C., 1873. A Treatise on Electricity and Magnetism. Clarendon Press, Oxford.

McCartney, L.N., Kelly, A., 2008. Maxwell's far-field methodology applied to the prediction of properties of multi-phase isotropic particulate composites. Proceedings of the Royal Society A: Mathematical, Physical and Engineering Sciences 464, 423–446.

McMillan, P.F., 2003. Chemistry of materials under extreme high pressure-high-temperature conditions. Chemical communications 919–23.

Menon, S.K., Martin, P.L., 1986. Determination of the anisotropy of surface free energy of fine metal particles. Ultramicroscopy 20, 93–98.

Miyazawa, T., Aratake, M., Onaka, S., 2012. Superspherical-shape approximation to describe the morphology of small crystalline particles having near-polyhedral shapes with round edges. Journal of Mathematical Chemistry 50, 249–260.

Mogilevskaya, G., Nikolskiy, D. V., 2015. The shape of Maxwell's equivalent inhomogeneityand "strange" properties of regular polygons and other symmetric domainss. Quarterly Journal of Mechanics and Applied Mathematics 68, 363–385.

Mori, T., Tanaka, K., 1973. Average stress in matrix and average elastic energy of materials with misfitting inclusions. Acta Metallurgica 21, 571–574.

MSC Software, 2012. MSC Marc 2012 User Documentation. Volume A: Theory and User Information.

Niu, W., Zheng, S., Wang, D., Liu, X., Li, H., Han, S., Chen, J., Tang, Z., Xu, G., 2009. Selective synthesis of single-crystalline rhombic dodecahedral, octahedral, and cubic gold nanocrystals. Journal of the American Chemical Society 131, 697–703.

Onaka, S., 2016. Extended Superspheres for Shape Approximation of Near Polyhedral Nanoparticles and a Measure of the Degree of Polyhedrality. Nanomaterials 6, 27.

Onaka, S., 2006. Simple equations giving shapes of various convex polyhedra: the regular polyhedra and polyhedra composed of crystallographically low-index planes. Philosophical Magazine Letters 86, 175–183.

Onaka, S., Kobayashi, N., Fujii, T., Kato, M., 2003. Energy analysis with a superspherical shape approximation on the spherical to cubical shape transitions of coherent precipitates in cubic materials. Materials Science and Engineering: A 347, 42–49.

Park, K.H., Jang, K., Kim, H.J., Son, S.U., 2007. Near-monodisperse tetrahedral rhodium nanoparticles on charcoal: The shape-dependent catalytic hydrogenation of arenes. Angewandte Chemie - International Edition 46, 1152–1155.

Rasool, A., Böhm, H.J., 2012. Effects of particle shape on the macroscopic and microscopic linear behaviors of particle reinforced composites. International Journal of Engineering Science 58, 21–34.

Saxena, N., Mavko, G., 2014. Exact equations for fluid and solid substitution. Geophysics 79.

Segurado, J., Llorca, J., 2002. A numerical approximation to the elastic properties of sphere-reinforced composites. Journal of the Mechanics and Physics of Solids 50, 2107–2121.

Seo, D., Ji, C.P., Song, H., 2006. Polyhedral gold nanocrystals with Oh symmetry: From octahedra to cubes. Journal of the American Chemical Society 128, 14863–14870.

Sevostianov, I., 2014. On the shape of effective inclusion in the Maxwell homogenization scheme for anisotropic elastic composites. Mechanics of Materials 75, 45–59.

Sevostianov, I., Chen, F., Giraud, A., Grgic, D., 2016. Compliance and resistivity contribution tensors of axisymmetric concave pores. International Journal of Engineering Science 101, 14–28.

Sevostianov, I., Giraud, A., 2012. On the Compliance Contribution Tensor for a Concave Superspherical Pore. International Journal of Fracture 177, 199–206.

Sevostianov, I., Kachanov, M., 1999. Compliance tensors of ellipsoidal inclusions.

International Journal of Fracture 96, 3–7.

Sevostianov, I., Kachanov, M., 2007. Relations between compliances of inhomogeneities having the same shape but different elastic constants. International Journal of Engineering Science 45, 797–806.

Sevostianov, I., Kachanov, M., Zohdi, T.I., 2008. On computation of the compliance and stiffness contribution tensors of non ellipsoidal inhomogeneities. International Journal of Solids and Structures 45, 4375–4383.

Sun, S., Yang, Z., 2014. Recent advances in tuning crystal facets of polyhedral cuprous oxide architectures. RSC Adv. 4, 3804–3822.

Sundquist, B.E., 1964. A direct determination of the anisotropy of the surface free energy of solid gold, silver, copper, nickel, and alpha and gamma iron. Acta Metallurgica 12, 67–86.

Tsukrov, I., Novak, J., 2002. Effective elastic properties of solids with defects of irregular shapes. International Journal of Solids and Structures 39, 1539–1555.

Tsukrov, I., Novak, J., 2004. Effective elastic properties of solids with two-dimensional inclusions of irregular shapes. International Journal of Solids and Structures 41, 6905–6924.

Walpole, L.J., 1969. On the overall elastic moduli of composite materials. Journal of the Mechanics and Physics of Solids 17, 235–251.

Wang, Z.L., 2000. Transmission Electron Microscopy of Shape-Controlled Nanocrystals and Their Assemblies. The Journal of Physical Chemistry B 104, 1153–1175.

Wu, T. Te, 1966. The effect of inclusion shape on the elastic moduli of a two-phase material. International Journal of Solids and Structures 2, 1–8.

Zeon Han, S., Kim, K.H., Kang, J., Joh, H., Kim, S.M., Ahn, J.H., Lee, J., Lim, S.H., Han, B., 2015. Design of exceptionally strong and conductive Cu alloys beyond the conventional speculation via the interfacial energy-controlled dispersion of γ-Al2O3 nanoparticles. Scientific Reports 5, 17364.

Zimmerman, R.W., 1986. Compressibility of Two-Dimensional Cavities of Various Shapes. Journal of Applied Mechanics 53, 500–504.

Zohdi, T.I., 2001. Computational optimization of the vortex manufacturing of advanced materials. Computer Methods in Applied Mechanics and Engineering 190, 6231–6256.

Zohdi, T.I., 2003a. Constrained inverse formulations in random material design. Computer Methods in Applied Mechanics and Engineering 192, 3179–3194.

Zohdi, T.I., 2003b. Genetic design of solids possessing a random-particulate microstructure. Philosophical Transactions of the Royal Society A: Mathematical, Physical and Engineering Sciences 361, 1021–1043.

Zohdi, T.I., Wriggers, P., eds., 2005. An Introduction to Computational Micromechanics. Springer Berlin Heidelberg, Berlin, Heidelberg.